Chinese Chemical Letters 33 (2022) 247–251

Contents lists available at ScienceDirect

Chinese Chemical Letters

journal homepage: www.elsevier.com/locate/cclet

Two star-shaped small molecule donors based on benzodithiophene unit for organic solar cells

Jun Xu[a,c], Jinsheng Zhang[a,b], Daobin Yang[a,b,*], Kuibao Yu[a], Dandan Li[a,b], Zihao Xia[a], Ziyi Ge[a,b,*]

[a] Ningbo Institute of Materials Technology and Engineering, Chinese Academy of Sciences, Ningbo 315201, China
[b] Center of Materials Science and Optoelectronics Engineering, University of Chinese Academy of Sciences, Beijing 100049, China
[c] Nano Science and Technology Institute, University of Science and Technology of China, Suzhou 215123, China

ARTICLE INFO

Article history:
Received 28 April 2021
Revised 4 June 2021
Accepted 7 June 2021
Available online 15 June 2021

Keywords:
Star-shaped molecules
Benzodithiophene
Suzuki coupling
Donor materials
Small molecules
Organic solar cells

ABSTRACT

Star-shaped small molecules have attracted great attention for organic solar cells (OSCs) because they have three-dimensional charge-transport characteristics, strong light absorption capacities and easily tunable energy levels. Herein, three- and four-armed star-shaped small molecule donors, namely BDT-3Th and BDT-4Th, respectively, have been successfully designed and synthesized, which used benzodithiophene (BDT) as the central unit. The two star-shaped intermediates (**2a** and **2b**) could be simultaneously obtained by one-step of Suzuki coupling, and 1,2-dimethoxyethane played a key role in the Suzuki coupling. Both of them have excellent thermal stability, good solubility and broad absorption. Four-armed BDT-4Th shows a slightly higher extinction coefficient, a deeper HOMO energy level and an obviously better phase separation morphology when blended with Y6 than three-armed BDT-3Th. As a result, increased power conversion efficiency (PCE) of 5.83% is obtained in the BDT-4Th:Y6-based OSC devices, which is obviously higher than that of the BDT-3Th:Y6-based devices (PCE = 3.78%). To the best of our knowledge, this is the highest PCE among the BDT-based star-shaped donors-based OSCs. This result provides an effective strategy to obtain star-shaped small molecule donor materials for high efficient organic solar cells.

Owing to the properties of light-weight, flexibility and the ability of large-area fabrication, solution-processed organic solar cells (OSCs) have been extensively investigated in the past few decades [1–4]. Currently, the power conversion efficiency (PCE) of the OSCs based on polymer as donors and non-fullerene molecules as acceptors has reached over 18% [5–8]. Nevertheless, in comparison with polymer materials, small-molecule materials, which have the advantages of definite molecular structure, easy separation and purification, and good batch-to-batch reproducibility, have aroused great interest for the OSC application [9–13]. Up to date, the PCE of all small molecules OSCs (ASM-OSCs) was up to 15%, indicating a promising future [14–16].

Recently, star-shaped small molecules have attracted great attention for OSCs because they have three-dimensional charge-transport characteristics, strong light absorption capacities and easily tunable energy levels [17–19]. Numerous star-shaped small molecule acceptors have been successfully developed, the PCE of the OSC devices based on that has exceeded 10% [20,21]. In 2017, H. Yan *et al.* reported a star-shaped acceptor FTTB-PDI4 bearing a cross-like core tetrathienylbenzene (TTB) and four end-cappers perylenediimides (PDIs), and a high PCE of 10.5% in the P3TEA:FTTB-PDI4-based OSC device was achieved [20]. However, few works focused on star-shaped small molecule donors, the highest PCE of the OSC device was only 7.4% so far [22]. Remarkably, benzodithiophene (BDT) is a great unit for constructing high-performance donor materials owing to the large planar conjugated structure [23,24]. L. Yu and C. Yang *et al.* reported some star-shaped acceptors using BDT as the central unit and four PDIs as end-cappers, all of the PCEs of their OSC devices exceeded 8% [25,26]. However, recently, M. Heeney *et al.* developed a star-shaped donor BDT(DPP)$_4$, containing a cross-like core BDT and four end-cappers diketopyrrolopyrrole (DPP), and the BDT(DPP)$_4$:PC$_{71}$BM and BDT(DPP)$_4$:C$_8$-ITIC-based OSC devices exhibited only 2.5% and 3.9% of efficiency, respectively [27]. Therefore, it is a great challenge to develop high-performance BDT-based star-shaped donors for organic solar cells.

* Corresponding authors.
E-mail addresses: yangdaobin@nimte.ac.cn (D. Yang), geziyi@nimte.ac.cn (Z. Ge).

https://doi.org/10.1016/j.cclet.2021.06.023
1001-8417/

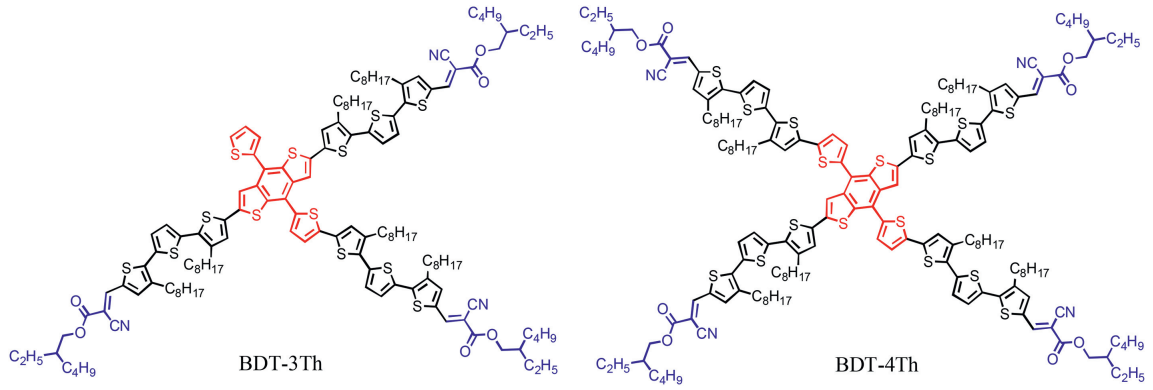

Scheme 1. Chemical structures of the BDT-3Th and BDT-4Th.

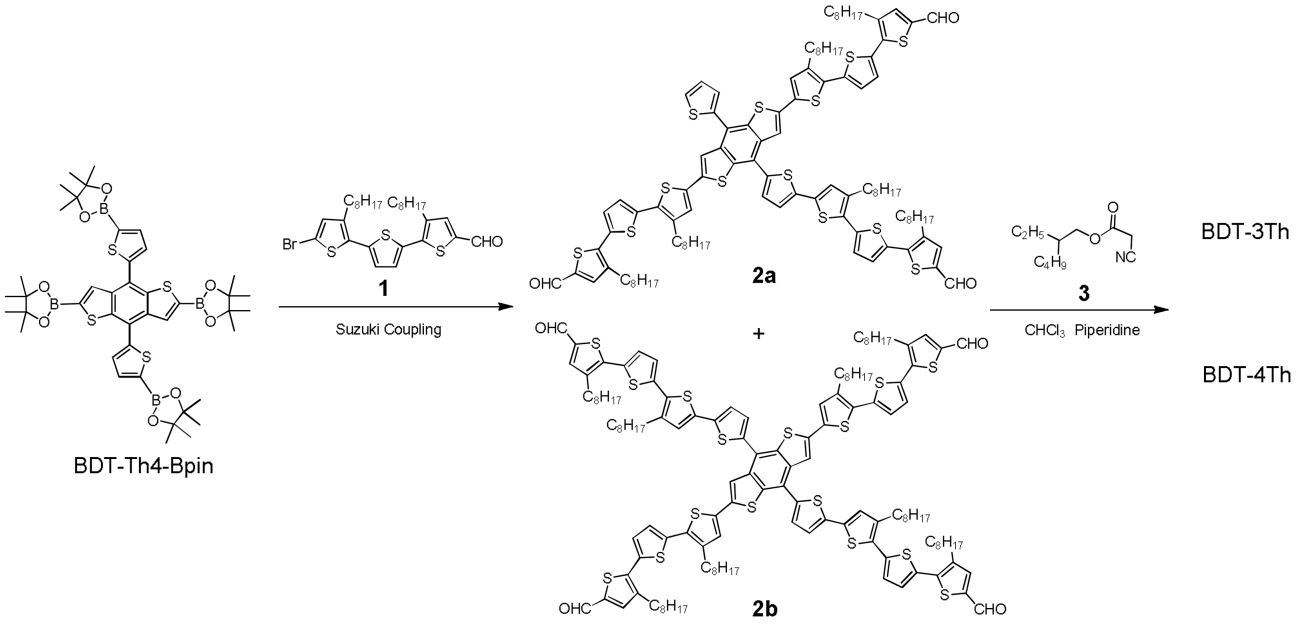

Scheme 2. Synthesis routes of the BDT-3Th and BDT-4Th.

Herein, two A-π-D-π-A type star-shaped small molecule donors BDT-3Th and BDT-4Th using BDT as the cross-like electron-donor units, 3,3′′-dioctyl-2,2′:5′,2′′-terthiophene as the π-bridge units and 2-ethylhexyl cyanoacetate as the electron-acceptor units, have been successfully designed and synthesized, as shown in Scheme 1. BDT-3Th and BDT-4Th correspond to three-armed and four-armed compounds, respectively. Compared with three-armed BDT-3Th, four-armed BDT-4Th displays a relatively blue-shifter absorption spectrum, but shows a higher extinction coefficient, a deeper HOMO energy level and an obviously better phase separation morphology when blended with Y6 (the chemical structure are shown in Fig. S1 in Supporting information) [28]. As a result, the PCE of 5.83% with an open-circuit voltage (V_{oc}) of 0.84 V, a fill factor (FF) of 0.402 and a short-circuit current density (J_{sc}) of 17.2 mA/cm^2 for the BDT-4Th:Y6-based OSC device was achieved, which is significantly higher than that of the BDT-3Th:Y6-based device (V_{oc} = 0.87 V, FF = 0.365, J_{sc} = 11.9 mA/cm^2, PCE = 3.78%). The effect of different number of arms on the optoelectronic properties of star-shaped small molecules has been carefully investigated.

The synthetic routes of BDT-3Th and BDT-4Th are depicted in Scheme 2. The detailed synthetic procedures are described in Supporting information. As we know, almost of the star-shaped molecules were synthesized *via* Suzuki coupling reaction with a common condition of $Pd_2(dba)_3$/(*p*-MeOPh)$_3$P or $Pd(PPh_3)_4$, K_2CO_3 aqueous solution and tetrahydrofuran (THF) [17]. Taking this condition, BDT-based star-shaped molecules were successfully synthesized *via* Suzuki coupling between BDT-Th-4Bpin with 4 equiv. of monobrominated PDI or DPP units with good yields of over 40% [25–27]. However, when we took the above condition on the Suzuki coupling between BDT-Th4-Bpin and compound **1**, compounds **2a** or **2b** could not be observed in the reaction mixture by thin layer chromatography (TLC) analysis. We tried to extend the reaction time, but failed. Finally, the different organic solvents, such as toluene, *N,N*-dimethylformamide (DMF) and 1,2-dimethoxyethane, were used for the Suzuki coupling. As shown in Table 1, only using 1,2-dimethoxyethane as solvent, compounds **2a** or **2b** were observed. After careful separation and purification, five compounds were obtained at the same time, the corresponding

Table 1
The overview of the reaction results under different solvents.

No.	Different conditions	TLC
1	$Pd_2(dba)_3$/(*p*-MeOPh)$_3$P/2 mol/L K_2CO_3/THF	No
2	$Pd_2(dba)_3$/(*p*-MeOPh)$_3$P/2 mol/L K_2CO_3/Toluene	No
3	$Pd_2(dba)_3$/(*p*-MeOPh)$_3$P/2 mol/L K_2CO_3/DMF	No
4	$Pd_2(dba)_3$/(*p*-MeOPh)$_3$P/2 mol/L K_2CO_3/1,2-dimethoxyethane	Observed

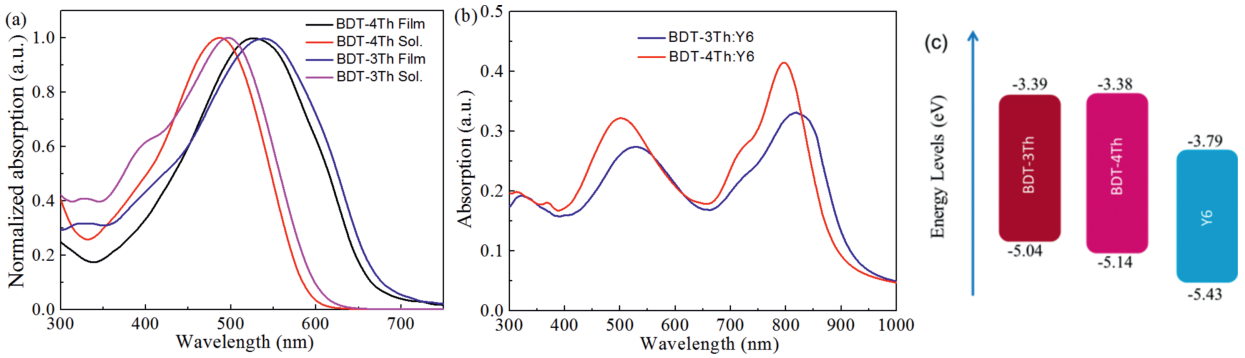

Fig. 1. UV–vis absorption spectra of BDT-3Th and BDT-4Th in thin film and in dilute solutions (a), BDT-3Th:Y6 and BDT-4Th:Y6 blend films (b), and the energy level diagrams of the BDT-3Th, BDT-4Th and Y6 (c).

Table 2
Optical and electrochemical properties of the BDT-3Th and BDT-4Th.

Donors	Absorption λ_{max} (nm)		E_g^{opt}	E_{HOMO}	E_{LUMO}
	Solution (L mol^{-1} cm^{-1})	Film	(eV)	(eV)	(eV)
BDT-3Th	497 (1.43 × 10^5)	539	1.97	−5.04	−3.39
BDT-4Th	487 (1.83 × 10^5)	529	2.01	−5.14	−3.38

chemical structures are shown in Table S1 (Supporting information). Among them, the three-armed compound **2a** and four-armed compound **2b** were obtained with yields of 16% and 18%, respectively. The low yields are attributed to the existence of other three by-products, their chemical structures are shown in Table S1. Finally, the BDT-3Th and BDT-4Th were synthesized *via* Knoevenagel condensation reaction with yields of 31% and 60%, respectively. The objective molecular structures were characterized by ^{1}H NMR, time of flight mass (TOF-MS) spectrometer. Both of the BDT-3Th and BDT-4Th can be soluble in chloroform (CF) and chlorobenzene (CB), which could satisfy the needs of device fabrication requirements, however BDT-4Th has an obviously higher solubility than BDT-3Th (Table S2 in Supporting information). As shown in Fig. S2 (Supporting information), the thermal decomposition temperatures of BDT-3Th and BDT-4Th are as high as 371 °C and 375 °C, respectively. This indicates that both the two molecules have an excellent thermal stability and could well meet the requirements of temperature conditions for device preparation.

The UV–vis absorption spectra of BDT-3Th and BDT-4Th in thin films and solutions are shown in Fig. 1a, and the corresponding data are summarized in Table 2. In both dilute solutions and thin films, the absorption maximum of BDT-4Th is blue-shifted by 10 nm from that of BDT-3Th, because the π-conjugated system of BDT-3Th has a smaller twist between the thiophene ring and the BDT core (10° *vs.* 12°, as shown in Fig. S3 in Supporting information) than that of BDT-4Th, leading to a more planar conjugation systems of BDT-3Th. Nevertheless, BDT-4Th has a higher molar extinction coefficient of 1.83 × 10^5 L mol^{-1} cm^{-1} than BDT-3Th (ε = 1.43 × 10^5 L mol^{-1} cm^{-1}). Compared to the absorption spectra in solution, the absorption spectra of BDT-3Th and BDT-4Th are both red-shifted by around 40 nm owing to the strong π-π intermolecular interactions in the thin films [29]. The absorption edges of BDT-3Th and BDT-4Th thin films are 630 nm and 618 nm, respectively, corresponding to the medium optical bandgaps of 1.97 and 2.01 eV. As shown in Fig. 1b, when blended with non-fullerene acceptor Y6, both of the blend films present a very broad absorption spectra over the 300–900 nm range. The BDT-3Th:Y6 film exhibits a broader absorption spectra, however, the absorption intensity is obviously lower than that of BDT-4Th:Y6 film. Consequently, the BDT-4Th:Y6 film can harvest more sun light, which may have great influence on the generation of higher J_{sc}.

Cyclic voltammetry (CV) was measured to estimate the HOMO and LUMO energy levels of BDT-3Th and BDT-4Th. As shown in Fig. S4 (Supporting information), the HOMO/LUMO energy levels of BDT-3Th and BDT-4Th are calculated to be −5.04/−3.39 eV and −5.14/−3.38 eV, respectively. Relative to BDT-3Th, the HOMO energy level of BDT-4Th is 0.1 eV deeper, hence higher V_{oc} may be observed in the corresponding OSC devices [30]. In addition, the HOMO and LUMO energy levels of Y6 are calculated to be –5.43 and –3.79 eV, respectively [31]. Fig. 1c clearly shows that HOMO and LUMO energy levels of the two materials can match well with Y6, which are beneficial for exciton dissociation and charge separation [32]. As shown in Fig. S5 (Supporting information), BDT-3Th and BDT-4Th films present a strong fluorescence emission with the maximum peak of 690 and 680 nm, respectively. When blended with the non-fullerene acceptor Y6, both of the fluorescence emissions are quenched well. It is indicated that both of them possess an efficient charge transfer and charge separation [33,34].

A normal device structure with ITO/PEDOT:PSS/active layer/PDINO/Al was fabricated to investigate the photovoltaic properties of BDT-3Th and BDT-4Th [35]. The active layers are optimized by carefully varying the blend ratios of the donor and acceptor (D:A, weight ratio), and thermal annealing temperatures, the photovoltaic performances are summarized in Table S3 (Supporting informaiton). The *J-V* curve of the device under the optimized condition and the corresponding external quantum efficiency (EQE) curves are shown in Fig. 2, and the corresponding data as summarized in Table 3. The BDT-3Th:Y6-based OSCs device exhibits a PCE of 3.78% with a V_{oc} of 0.87 V, a J_{sc} of 11.9 mA/cm^2, and a FF of 0.365. While the BDT-4Th:Y6-based OSCs device displays an enhanced PCE of 5.83% with a V_{oc} of 0.84 V, a high J_{sc} of 17.2 mA/cm^2, and a FF of 0.403. The enhanced PCE is ascribed to the obviously higher J_{sc} and FF as compared to the BDT-3Th:Y6-based device. To explain the origin of the higher J_{sc}, the EQE spectra of the devices were measured, as shown in Fig. 2b. The much increased EQE values are observed in BDT-4Th:Y6-based devices from 350 nm to 950 nm range, thereby resulting in the high J_{sc}.

The surface morphologies of the BDT-3Th:Y6 and BDT-4Th:Y6 blend films were measured by atomic force microscopy (AFM). As shown in Fig. 3, both of the BDT-3Th:Y6 and BDT-4Th:Y6 blend films show a smooth surface morphology with a similar root-mean-square (RMS) roughness of around 0.50 nm. However, in comparison to the BDT-3Th:Y6 blend film, the BDT-4Th:Y6 blend film has a more clearly continuous interpenetrating network. Besides, we noted that there are lots of black particles appeared on the BDT-3Th:Y6 blend film, which may be attributed to the poor solubility of the BDT-3Th, thereby leading to poor miscibility with

Table 3
Photovoltaic parameters of the BDT-3Th:Y6 and BDT-4Th:Y6-based OSC devices with D:A ratio of 1:1.

Active layer [a]	V_{oc} (V)	J_{sc} (mA/cm^2)	J_{sc}^{EQE} (mA/cm^2)	FF	PCE (%) [b]
BDT-3Th:Y6	0.87 (0.85 ± 0.02)	11.9 (11.7 ± 0.2)	11.4 (11.2 ± 0.3)	0.365 (0.350 ± 0.020)	3.78 (3.50 ± 0.24)
BDT-4Th:Y6	0.84 (0.84 ± 0.01)	17.2 (17.0 ± 0.2)	16.6 (16.4 ± 0.2)	0.403 (0.396 ± 0.014)	5.83 (5.60 ± 0.20)

[a] The active layers were thermal annealed at 100 °C for 10 min.
[b] The average values are calculated from 10 cells.

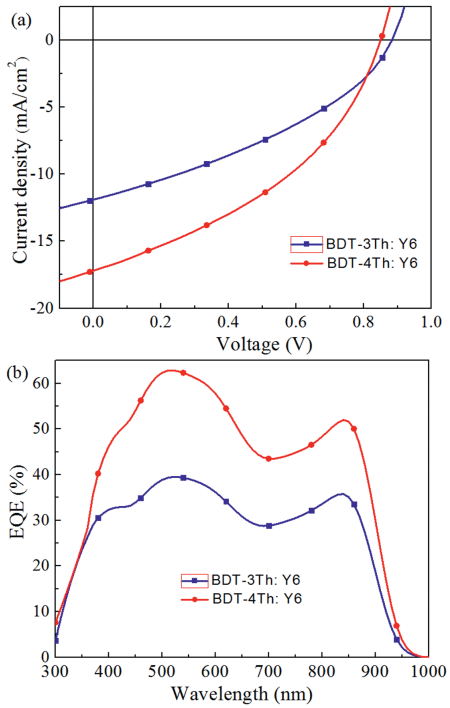

Fig. 2. *J-V* curves (a) and EQE curves (b) of the BDT-3Th:Y6 and BDT-4Th:Y6-based OSC devices.

Y6. Consequently, the phase separation behavior of BDT-4Th:Y6 blend film is obviously better than that of BDT-3Th:Y6 blend film, which is beneficial for charge transport, resulting in the higher J_{sc} and FF of BDT-4Th:Y6-based device. Grazing-incidence wide-angle X-ray scattering (GIWAXS) measurements were utilized to investigate the molecular packing and orientation of the BDT-3Th:Y6 and BDT-4Th:Y6 blend films. The 2D GIWAXS images and the corresponding plots in the in-plane (IP) and out-of-plane (OOP) directions are given in Fig. 3 and Fig. S6 (Supporting information). Both of the blend films display a clearly feature comprising of face-on and edge-on crystalline orientations [36,37]. However, the BDT-4Th:Y6 blend film exhibits an obviously stronger (010) π-π stacking peak at ~1.71 Å^{-1} (d = 3.64 Å) in the OOP direction than that of the BDT-3Th:Y6 blend film, which is beneficial for promoting charge transport and reducing charge recombination. Consequently, the enhanced J_{sc} and FF of the BDT-4Th:Y6-based OSC device could be observed.

In summary, two novel star-shaped small-molecule donors, three-armed BDT-3Th and four-armed BDT-4Th, have been successfully developed for organic solar cells. The two star-shaped intermediates (**2a** and **2b**) can be simultaneously obtained via one-step of the Suzuki coupling. It is worth noting that 1,2-dimethoxyethane plays a key role in the Suzuki coupling. Although three-armed BDT-3Th has a relatively red-shift absorption spectrum, four-armed BDT-4Th exhibits a higher extinction coefficient, a deeper HOMO energy level and a much better phase separation morphology when blended with Y6 than that of BDT-3Th, resulting in clearly higher J_{sc} and FF of the corresponding OSC devices. As a result, the PCE of the BDT-4Th:Y6-based OSC device is 5.83%, which is obviously higher than that of the BDT-3Th:Y6-based device (3.78%). Despite the PCE of absolute values are still low, we hope this work can help chemists understand the relationship between star-shaped small molecule donors and photoelectric performance, and expect promising properties in the future.

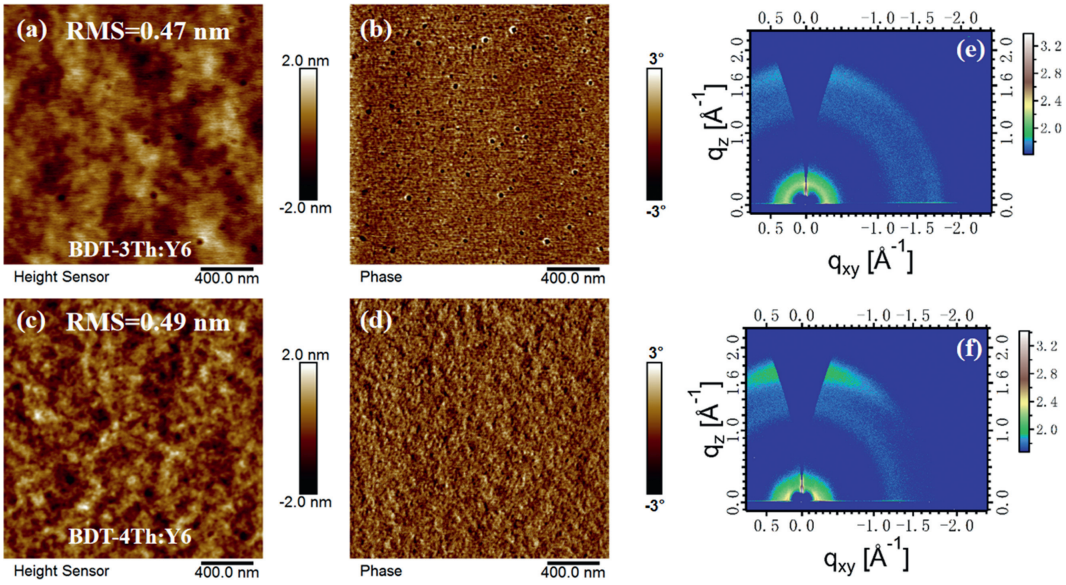

Fig. 3. AFM images for the BDT-3Th:Y6 (a, b) and BDT-4Th:Y6 (c, d) blend films, 2D GIWAXS images of the BDT-3Th:Y6 (e) and BDT-4Th:Y6 (f) blend films.

Declaration of competing interest

The authors declare that they have no known competing financial interests or personal relationships that could have appeared to influence the work reported in this paper.

Acknowledgments

We acknowledge the financial support for this work by the National Science Fund for Distinguished Young Scholars (No. 21925506), National Natural Science Foundation of China (No. 51773212), Ningbo S&T Innovation 2025 Major Special Program (No. 2018B10055).

Supplementary materials

Supplementary material associated with this article can be found, in the online version, at doi:10.1016/j.cclet.2021.06.023.

References

[1] O. Inganas, Adv. Mater. 30 (2018) 1800388.
[2] S. Park, T. Kim, S. Yoon, et al., Adv. Mater. 32 (2020) 2002217.
[3] X. Xu, G. Zhang, Y. Li, et al., Chin. Chem. Lett. 30 (2019) 809–825.
[4] L. Shao, F. Tong, M. Zhu, et al., Chin. Chem. Lett. 31 (2020) 2452–2458.
[5] Q. Liu, Y. Jiang, K. Jin, et al., Sci. Bull. 65 (2020) 272–275.
[6] Y. Lin, M.I. Nugraha, Y. Firdaus, et al., ACS Energy Lett. 5 (2020) 3663–3671.
[7] L. Zhan, S. Li, X. Xia, et al., Adv. Mater. 33 (2021) 2007231.
[8] M. Zhang, L. Zhu, G. Zhou, et al., Nat. Commun. 12 (2021) 309.
[9] D. Yang, H. Sasabe, T. Sano, et al., ACS Energy Lett. 2 (2017) 2021–2025.
[10] Q. Wei, W. Liu, M. Leclerc, et al., Sci. China Chem. 63 (2020) 1352–1366.
[11] W. Ye, Y. Yang, Z. Zhang, et al., Solar RRL 4 (2020) 2000258.
[12] J. Gao, J. Ge, R. Peng, et al., J. Mater. Chem. A 8 (2020) 7405–7411.
[13] Y. Chang, J. Li, Y. Chang, et al., Chin. Chem. Lett. 32 (2021) 2904–2908.
[14] D. Hu, Q. Yang, H. Chen, et al., Energy Environ. Sci. 13 (2020) 2134–2141.
[15] J. Qin, C. An, J. Zhang, et al., Sci. China Mater. 63 (2020) 1142–1150.
[16] L. Nian, Y. Kan, K. Gao, et al., Joule 4 (2020) 2223–2236.
[17] Y.Q. Pan, G.Y. Sun, ChemSusChem 12 (2019) 4570–4600.
[18] H. Wang, M. Li, Y. Liu, et al., J. Mater. Chem. C 7 (2019) 819–825.
[19] X. Gao, Y. Wu, X. Song, et al., Dyes Pigments 188 (2021) 109216.
[20] J. Zhang, Y. Li, J. Huang, et al., J. Am. Chem. Soc. 139 (2017) 16092–16095.
[21] G. Cai, W. Wang, J. Zhou, et al., ACS Mater. Lett. 1 (2019) 367–374.
[22] H. Wang, Q. Yue, T. Nakagawa, et al., J. Mater. Chem. A 7 (2019) 4072–4083.
[23] L. Ye, S. Zhang, L. Huo, et al., Acc. Chem. Res. 47 (2014) 1595–1603.
[24] H. Yao, L. Ye, H. Zhang, et al., Chem. Rev. 116 (2016) 7397–7457.
[25] Q. Wu, D. Zhao, A.M. Schneider, et al., J. Am. Chem. Soc. 138 (2016) 7248–7251.
[26] Z. Luo, T. Liu, W. Cheng, et al., J. Mater. Chem. C 6 (2018) 1136–1142.
[27] Q. He, M. Shahid, J. Panidi, et al., J. Mater. Chem. C 7 (2019) 6622–6629.
[28] J. Yuan, Y. Zhang, L. Zhou, et al., Joule 3 (2019) 1140–1151.
[29] D. Yang, H. Sasabe, Y. Jiao, et al., J. Mater. Chem. A 4 (2016) 18931–18941.
[30] N.K. Elumalai, A. Uddin, Energy Environ. Sci. 9 (2016) 391–410.
[31] D. Yang, K. Yu, J. Xu, et al., J. Mater. Chem. A 9 (2021) 10427–10436.
[32] M.C. Scharber, D. Mühlbacher, M. Koppe, et al., Adv. Mater. 18 (2006) 789–794.
[33] G. Yu, J. Gao, J.C. Hummelen, et al., Science 270 (1995) 1789–1791.
[34] N.S. Sariciftci, L. Smilowitz, A.J. Heeger, et al., Science 258 (1992) 1474–1476.
[35] T. Yan, W. Song, J. Huang, et al., Adv. Mater. 31 (2019) 1902210.
[36] T. Kumari, S.M. Lee, S.H. Kang, et al., Energy Environ. Sci. 10 (2017) 258–265.
[37] H. Bin, Y. Yang, Z.G. Zhang, et al., J. Am. Chem. Soc. 139 (2017) 5085–5094.